Probing Solute-Entrainer Interactions in Matrix-Modified Supercritical CO_2

JoAnn Zagrobelny and Frank V. Bright*

Contribution from the Department of Chemistry, Acheson Hall, State University of New York at Buffalo, Buffalo, New York 14214. *Received June 25, 1992*

Abstract: Binary supercritical fluids composed of CO_2 and small amounts of acetonitrile or methanol (entrainers) are studied as a function of fluid density, using pyrene as the solute probe. These experiments show how preferential entrainer clustering effects pyrene excimer formation. To this end, steady-state and time-resolved fluorescence spectroscopy are used in concert to probe the ground and excited states of pyrene. Results show that entrainers enhance solute–solvent clustering and slow the, traditionally diffusion-controlled, excimer formation reaction. Clustering also helps shield the excimer from non-radiative deactivation processes as evidenced by a longer decay time in the near-critical region. All data over our concentration range are consistent with a homogeneous pyrene ground state. There is no evidence for solute–solute (pyrene–pyrene) interactions prior to excitation. However, once in the excited state, excimer formation is facilitated due to the decreased fluid viscosity compared to liquids.

Introduction

The characteristic critical point for any chemical system is defined by its critical temperature (T_c) and pressure (P_c). Immediately below these points exists an equilibrium between the liquid and gaseous phases. Above the critical point the two phases coalesce into a supercritical fluid.[1] One unique feature of supercritical fluids is that the solvent characteristics are variable over a wide range.[2] For example, in the rear-critical region one can use temperature and pressure to adjust density from gas-like to liquid-like. However, the transport properties (i.e., diffusivity and viscosity) remain more on the order of a gas.[1-3] Thus, supercritical solvents possess enhanced solvating power compared to gases and improved mass transport compared to liquids.[1-3]

During this past decade, the unique characteristics of supercritical fluids have been used widely to effect separations and extractions.[3-7] More recent work has shown that supercritical fluids can be used as novel reaction media.[1b,8-14] On the basis of the well-know fact that solvents can affect reaction kinetics,[15] the tunability of supercritical fluids provides, in principle, a convenient way to control chemical reactions without changing the molecular structure of the solvent. However, to fully realize the potential of supercritical fluids, it becomes necessary to understand the molecular interactions and the system phase behavior. To this end, chemists and engineers have investigated various solute–supercritical fluid systems.

Erlich[16] first observed negative partial molar volumes for polar solutes in supercritical fluids. This anomalous result lead to more detailed thermodynamic measurements[17-19] (e.g., solubility and partial molar properties at infinite dilution) in supercritical fluids. For example, Eckert et al.[18,19] recovered partial molar volumes which were large and negative (approximately 100 times the bulk solvent molar volume) in the near-critical region. These experiments suggested an augmentation of solvent molecules about the solute at infinite dilution. This eventually lead to the idea that the fluid composition in the cybotactic region was enriched relative to the bulk—the so called clustering phenomena. Following from these experiments several groups have used molecular dynamics simulations and modeling[20-29] and spectroscopy[21,22,30-42] to probe this clustering phenomena.

Debenedetti et al.[24,25] qualitatively described these solute–fluid interactions for three limiting cases: attractive, weakly attractive, or repulsive. Each case was characterized by solute–solvent partial molar volume, enthalpy, and correlation length fluctuations. Solute–fluid clustering was apparent only in the attractive case.[24,25] More recent results[26] predict a dynamical solute–fluid cluster. Cochran et al.[28,29] calculated pair correlation functions and fluctuation integrals for supercritical systems using integral equation theories. Near the critical point, these authors observed the growth of the solute–solvent fluctuation integral resulting from an increase in the correlation length of the density fluctuations.

* Author to whom all correspondence should be addressed.

(1) (a) Reid, R. C.; Prausnitz, J. M.; Poling, B. E. *The Properties of Gases and Liquids*, 4th ed.; McGraw-Hill: New York, 1987. (b) *Supercritical Fluid Technology—Reviews in Modern Theory and Applications*; Bruno, T. J., Ely, J. F., Eds.; CRC Press: Boca Raton, FL, 1991.

(2) McHugh, M. A.; Krukonis, V. J. *Supercritical Fluid Extraction—Principles and Practice*: Butterworths: Boston, MA, 1986.

(3) Klesper, E. *Angew. Chem., Int. Ed. Engl.* **1978**, *17*, 738.

(4) Novotny, M. V.; Springston, S. R.; Peaden, P. A.; Fjeldstad, J. C.; Lee, M. L. *Anal. Chem.* **1981**, *53*, 407A.

(5) *Supercritical Fluid Chromatography*; Smith, R. M., Ed.; Royal Society of Chemistry Monograph: London, 1988.

(6) Berger, T. A.; Deye, J. F. *J. Chromatogr. Sci.* **1991**, *29*, 141.

(7) Brennecke, J. F.; Eckert, C. A. *AlChE J.* **1989**, *35*, 1409.

(8) *Supercritical Fluid Technology—Theoretical and Applied Approaches in Analytical Chemistry*; Bright, F. V., McNally, M. E., Eds.; ACS Symp. Ser. 488; American Chemical Society: Washington, DC, 1992; Chapter 1.

(9) Fulton, J. L.; Yee, G. G.; Smith, R. D. *J. Am. Chem. Soc.* **1991**, *113*, 8327.

(10) Howdle, S. M.; Healy, M. A.; Poliakoff, M. *J. Am. Chem. Soc.* **1990**, *112*, 4804.

(11) Narayan, R.; Antal, M. J. *J. Am. Chem. Soc.* **1990**, *112*, 1927.

(12) Erickson, J. C.; Schyns, P.; Cooney, C. L. *AlChE J.* **1990**, *36*, 299.

(13) Nakamura, K.; Fujii, H.; Chi, Y. M.; Yano, T. *Ann. N.Y. Acad. Sci.* **1990**, *613*, 319.

(14) Nakamura, K. *Trends Biotechnol.* **1990**, *8*, 288.

(15) March, J. *Advanced Organic Chemistry*, 3rd ed.; Wiley-Interscience: New York, 1985.

(16) Ehrlich, P.; Fariss, R. *J. Phys. Chem.* **1969**, *73*, 1164.

(17) Wu, P. C.; Ehrlich, P. *AlChE J.* **1973**, *19*, 533.

(18) Eckert, C. A.; Ziger, D. H.; Johnston, K. P.; Ellison, T. K. *Fluid Phase Equilib.* **1983**, *14*, 167.

(19) Eckert, C. A.; Ziger, D. H.; Johnston, K. P.; Kim, S. *J. Phys. Chem.* **1986**, *90*, 2738.

(20) Debenedetti, P. G. *Chem. Eng. Sci.* **1987**, *42*, 2203.

(21) Kim, S.; Johnston, K. P. *Ind. Eng. Chem. Res.* **1987**, *26*, 1206.

(22) Kim, S.; Johnston, K. P. *AlChE J.* **1987**, *33*, 1603.

(23) Debenedetti, P. G.; Kumar, S. K. *AlChE J.* **1988**, *34*, 645.

(24) Debenedetti, P. G.; Mohamed, R. S. *J. Chem. Phys.* **1990**, *90*, 4528.

(25) Debenedetti, P. G.; Petsche, I. B.; Mohamed, R. S. *Fluid Phase Equilib.* **1989**, *52*, 347.

(26) Petsche, I. B.; Debenedetti, P. G. *J. Phys. Chem.* **1991**, *95*, 386.

(27) Petsche, I. B.; Debenedetti, P. G. *J. Chem. Phys.* **1989**, *91*, 7075.

(28) Cochran, H. D.; Lee, L. L. In *Supercritical Fluid Science and Technology*; Johnston, K. P., Penninger, J. M. L., Eds.; ACS Symp. Ser. 406; American Chemical Society: Washington, DC, 1989; Chapter 3.

(29) Cochran, H. D.; Lee, L. L.; Pfund, D. M. *Proc. Int. Symp. Supercritical Fluids* **1988**, 245.

(30) Johnston, K. P.; Kim, S.; Combs, J. In *Supercritical Fluid Science and Technology*; Johnston, K. P., Penninger, J. M. L., Eds.; ACS Symp. Ser. 406; American Chemical Society: Washington, DC, 1989; Chapter 5.

0002-7863/93/1515-701$04.00/0

These results[28,29] support clustering in attractive solute–solvent pairs and cavitation in repulsive systems. This work also suggests that solute–solvent clustering may enhance solute–solvent interactions.

Spectroscopic measurements provide a molecular-level view of solute–fluid interaction and support cluster formation.[21,22,30-42] For example, steady-state and time-resolved fluorescence studies of the solute 6-propionyl-2-(dimethylamino)naphthalene (PRODAN) in CF_3H show clear evidence for the formation of solute–fluid clusters.[33] Additional studies[34,35] show that in the near-critical region the local density of N_2O about PRODAN is approximately 2.5 times greater than the bulk. The average number of solvent molecules in the cluster has been determined experimentally,[34,35] and is in good agreement with many of the theoretical calculations (vide supra).[20-22] Additional fluorescence-based work[36] on the twisted intramolecular charge transfer (TICT) of (*N*,*N*-dimethylamino)benzonitrile (DMABN) and ethyl *p*-(*N*,*N*-dimethylamino)benzoate (DMAEB) in supercritical fluids has shown that solute–fluid clustering can occur even at a reduced density ($\rho_r = \rho_{exp}/\rho_c$) of 0.5.

Nonpolar polyaromatic hydrocarbons have also been used to probe solute–fluid and solute–solute interactions in supercritical solvents. Brennecke et al.[37,38] reported on the steady-state fluorescence of pyrene in supercritical CO_2, C_2H_4, and CF_3H. Pyrene emission exhibits several vibronic bands and is very useful for probing solute–solvent interactions. Specifically, the intensity of the 0–0 transition (I_1) is extremely solvent dependent[43,44] and increases with increasing solute–solvent interactions. In contrast, the third vibronic band intensity (I_3) shows little variance between solvents.[43,44] Thus, by following I_1/I_3 it is possible to probe solute–solvent interactions.[43-44] Brennecke et al. found that this ratio, as expected, increased with fluid density;[37,38] however, it is unusually large in the region near the critical point, indicating enhanced solute–fluid interactions, i.e., clustering. More recent results by Knutson et al.[45] compared the experimental clustering data to molecular dynamics simulations involving the first, second, and third solvation shells. These results showed that the observed density augmentation arose only from the first solvation shell.

The effects of pyrene concentration on its static emission have also been investigated in supercritical fluids.[37,38] The most intriguing aspect of these results is the appearance of an excimer-like emission at pyrene concentrations in the low micromolar range. On the basis of these results, it was proposed that the excimer was a manifestation of increased solute–solute (pyrene–pyrene) interactions. This concept has been further supported[47] by integral equation calculations based on molecular distribution functions using the correlation function for the Lennard-Jones mixture simulating both CO_2–naphthalene and CO_2–pyrene. These simulations feature increased height of the solute–solute pair distributions near the critical point and predict increased short-range solute concentration about a solute molecule.

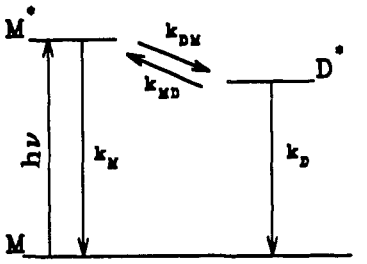

Figure 1. Energy-level diagram for pyrene excimer formation: $h\nu$, absorbed photon; k_M, de-excitation rate from monomer species; k_{DM}, bimolecular rate coefficient for formation of pyrene excimer; k_{MD}, unimolecular rate coefficient for dissociation of the pyrene excimer; and k_D, de-excitation rate from the excimer species.

Our most recent work[48,49] has centered on using the photophysics of pyrene in pure supercritical fluids to probe the kinetics of solute–fluid and solute–solute interactions. From steady-state and time-resolved fluorescence spectroscopy we concluded that the pyrene excimer is observed at micromolar concentrations in supercritical CO_2 and C_2H_4 because of (1) increased diffusivity and (2) fluid–excimer interactions which stabilize the excimer excited state. Thus, solute–fluid clusters do not affect the mechanism of excimer formation in CO_2 and C_2H_4; however, once formed in the excited state, they affect the excimer decay rate.[48,49] In contrast, pyrene excimer formation occurs in CF_3H because the apparent excited-state equilibrium constant favors excimer formation.[49] Here the recovered bimolecular rates for excimer production are slowed appreciably (compared to that predicted by diffusion control) as a consequence of enhanced solute–fluid interactions.[49]

The bulk of the work in supercritical fluid science and technology has used CO_2 as the solvent.[1,2] This is a result of its nontoxicity, low cost, nonflammability, and mild critical conditions (T_c = 31.04 °C, P_c = 72.85 atm, ρ_c = 0.468 g/cm^3).[2] Unfortunately, CO_2 alone does not dissolve polar solutes well, and even nonpolar solutes have limited solubility.[7] However, addition of small amounts (1–5 mol %) of relatively volatile entrainers (cosolvents) increases the solvent strength of CO_2[7] but does not significantly alter the critical properties or density compared to a pure fluid.[50] Thus, entrainers can improve the selectivity (i.e., the ability to extract solute in preference to another) of supercritical solvents. Spectroscopic methods have been used to show that these improvements can be described in terms of specific solute–entrainer interactions.[50-53]

In an effort to improve our understanding of solute–fluid clustering in entrainer-modified supercritical fluids, we have investigated their effect on pyrene excimer formation. Here we report on the density and temperature dependence of pyrene photophysics in binary supercritical fluids composed of CO_2 and acetonitrile or methanol. These results provide new information on entrainers in supercritical fluid clustering. Acetonitrile and

(31) Johnston, K. P.; Kim, S.; Wong, J. M. *Fluid Phase Equilib.* **1987**, *38*, 39.
(32) Hrnjez, B. J.; Yazdi, P. T.; Fox, M. A.; Johnston, K. P. *J. Am. Chem. Soc.* **1989**, *111*, 1915.
(33) Betts, T. A.; Zagrobelny, J.; Bright, F. V. *J. Supercrit. Fluids* **1992**, *5*, 48.
(34) Betts, T. A.; Zagrobelny, J.; Bright, F. V. *J. Am. Chem. Soc.* **1992**, *114*, 8163.
(35) Betts, T. A. Ph.D. Thesis, State University of New York at Buffalo, 1992.
(36) Sun, Y.-P.; Fox, M. A.; Johnston, K. P. *J. Am. Chem. Soc.* **1992**, *114*, 1187.
(37) Brennecke, J. F.; Eckert, C. A. In *Supercritical Fluid Science and Technology*; Johnston, K. P., Penninger, J. M. L., Eds.; ACS Sypm. Ser. 406; American Chemical Society: Washington, DC, 1989; Chapter 2.
(38) Brennecke, J. F.; Tomasko, D. L.; Peshkin, J.; Eckert, C. A. *Ind. Eng. Chem. Res.* **1990**, *29*, 1682.
(39) Brennecke, J. F.; Tomasko, D. L.; Eckert, C. A. *J. Phys. Chem.* **1990**, *94*, 7692.
(40) Ben-Amotz, D.; LaPlant, F.; Shea, D.; Gardecki, J.; List, D. In *Supercritical Fluid Technology—Theoretical and Applied Approaches in Analytical Chemistry*; Bright, F. V., McNally, M. E., Eds.; ACS Symp. Ser. 488; American Chemical Society: Washington, DC, 1992; Chapter 2.
(41) Blitz, J. P.; Yonker, C. R.; Smith, R. D. *J. Phys. Chem.* **1989**, *93*, 6661.
(42) Zerda, T. W.; Song, X.; Jonas, J. *Appl. Spectrosc.* **1986**, *40*, 1194.
(43) Dong, D. C.; Winnik, M. A. *Can. J. Chem.* **1984**, *62*, 2560.
(44) Kalyanasundaram, K.; Thomas, J. K. *J. Am. Chem. Soc.* **1977**, *99*, 2039.
(45) Knutson, B. L.; Tomasko, D. L.; Eckert, C. A.; Debenedetti, P. G., Chialvo, A. A. In *Supercritical Fluid Technology—Theoretical and Applied Approaches in Analytical Chemistry*; Bright, F. V., McNally, M. E., Eds.; ACS Symp. Ser. 488; American Chemical Society: Washington, DC, 1992; Chapter 5.
(46) Birks, J. B. *Photophysics of Aromatic Molecules*; Wiley-Interscience: New York, 1970.
(47) Wu, R.-S.; Lee, L. L.; Cochran, H. D. *Ind. Eng. Chem. Res.* **1990**, *29*, 977.
(48) Zagrobelny, J.; Betts, T. A.; Bright, F. V. *J. Am. Chem. Soc.* **1992**, *114*, 5249.
(49) Zagrobelny, J.; Bright, F. V. *J. Am. Chem. Soc.* **1992**, *114*, 7821.
(50) Dobbs, J. M.; Wong, J. M.; Johnston, K. P. *J. Chem. Eng. Data* **1986**, *31*, 303.
(51) Dobbs, J. M.; Wong, J. M.; Lahiere, R. J.; Johnston, K. P. *Ind. Eng. Chem. Res.* **1987**, *26*, 56.
(52) Dobbs, J. M.; Johnston, K. P. *Ind. Eng. Chem. Res.* **1987**, *26*, 1476.
(53) Lemert, R. M.; Johnston, K. P. *Ind. Eng. Chem. Res.* **1991**, *30*, 1222.

methanol also provide a convenient means to compare aprotic and protic entrainers.

Theory

In normal liquids, the kinetic model shown in Figure 1 describes the pyrene monomer and excimer emission process.[46] The species M, M*, and D* denote the ground-state monomer, excited-state monomer, and excited-state dimer (excimer), respectively. The terms k_M, k_D, k_{MD}, and k_{DM} represents the emissive rate coefficients for the monomer and excimer, the non-radiative unimolecular D* → M* + M (reverse) rate, and the non-radiative bimolecular M* + M → D* (forward) rate, respectively. The $h\nu$ symbolism denotes an absorption process that populates M* only; no D exists in the ground state.[46] The individual rate terms given in Figure 1 are recovered by simultaneous, global analysis of multiple fluorescence decay experiments.[54-57] That is, we analyze *simultaneously* the intensity decay traces from multiple wavelength and pyrene concentration experiments and recover the rate terms directly. The goodness-of-fit between the experimental data and the assumed model is judged by the reduced χ^2 (χ^2_r) residuals and autocorrelation function.[54] The theoretical treatment used to define the global algorithm can be found in ref 54.

From Einstein–Smoluchowski diffusion theory,[58] the bimolecular rate coefficient for a diffusion-controlled reaction is given by

$$k_{DM} = 8000RT/0.3\eta \qquad (1)$$

where R is the gas constant (J mol^{-1} K^{-1}), T is the temperature in Kelvin, and η is the fluid viscosity in poise. For pyrene excimer emission in normal liquids, the bimolecular rate (k_{DM}; M* + M → D*) generally follows this simple diffusion model.[46]

Experimental Section

Detailed information on the high-pressure apparatus and time-resolved instrumentation can be found elsewhere.[48] All steady-state fluorescence experiments were carried out using a SLM 48000 MHF spectrofluorometer (SLM Instruments) modified to accommodate the high-pressure optical cells.[59,60] In the current configuration, the temperature and pressure imprecision are 0.1 °C and 0.2 bar, respectively. At 450 W Xe-arc lamp serves as the excitation source, and monochromators are used for excitation and emission wavelength selection.

All time-resolved experiments were performed using an in-house constructed N_2 laser/boxcar-based system interfaced to a personal computer.[48] The control/acquisition BASIC software was developed and written in house. The time-resolved intensity decay data are analyzed using a commercially available software package (Globals Unlimited).

Sample Preparation. SFC grade CO_2 (<5 ppm O_2) was purchased from Scott Specialty Gases, pyrene (99%) was obtained from Aldrich, and acetonitrile and methanol (HPLC grade) are from Fisher. All reagents were used as received. Stock solutions of pyrene were prepared in absolute ethanol (Quantum).

To prepare a sample for study, a small aliquot of the stock pyrene solution (1 mM) is micropipeted into the optical cell (5 mL internal volume) and the solvent removed by gently heating (60 °C) the cell for several hours. After complete evaporation of the ethanol, the cell is connected to the high-pressure pump through a series of valves.[59] Residual O_2 is removed from the cell by maintaining a vacuum (50 μm Hg) for 10–15 min. An HPLC injector (Rheodyne 7010) is used to accurately introduce the entrainer (methanol or acetonitrile) into the system.[35] A vacuum is pulled through the injection port, then deoxygenated solvent (purged with N_2) is placed in the sample loop (5, 10, or 20 μL). To charge the cell, the pump head and optical cell are brought to the same temperature[59] to minimize temperature gradients, the cell is pre-pressurized, cosolvent is injected, and the system is raised to the desired pressure and equilibrated for 30 min. When density studies are performed the optical cell remains attached to the high-pressure pumping system and the pressure is adjusted as required (low → high). In a given experiment, the molar concentration of pyrene and cosolvent remain constant. The density (ρ) and viscosity of CO_2 were obtained directly from the literature.[61,62]

Because the cluster process occurs most strongly in the highly compressible region about the critical point,[2] we have investigated this region in detail (Figure 2).

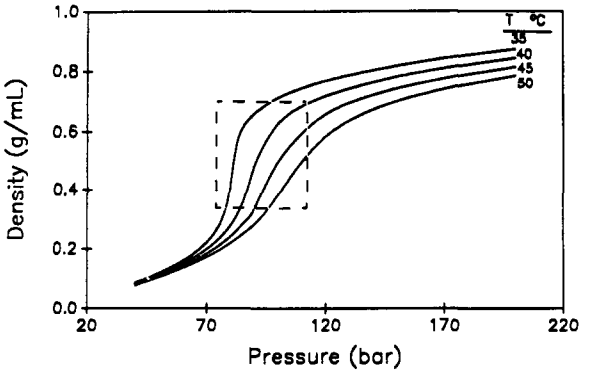

Figure 2. Isotherms for CO_2. The area contained within the dashed box indicates the region over which experiments were carried out.

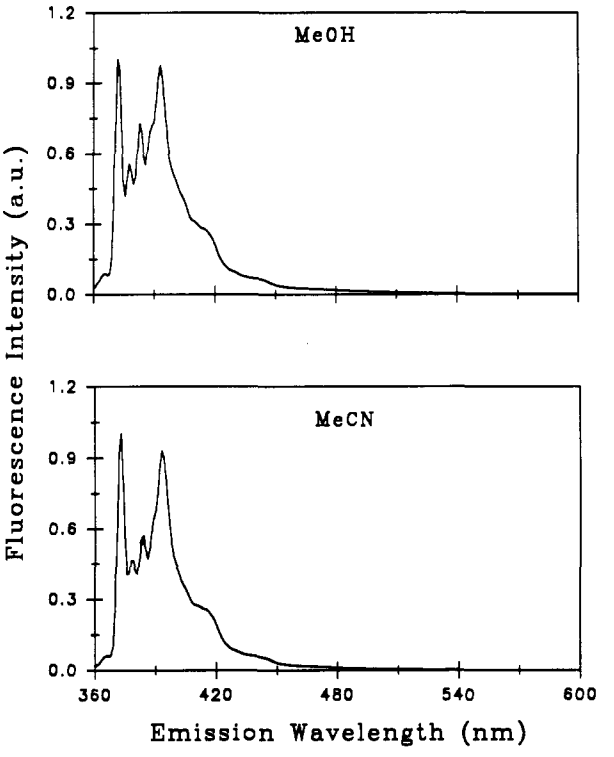

Figure 3. Steady-state emission spectra for 100 μM pyrene in liquid methanol (upper panel) and acetonitrile (lower panel). λ_{ex} = 337 nm; excitation spectral bandpass = 16 nm; emission spectral bandpass = 2 nm.

Results and Discussion

Steady-State Experiments. Figure 3 shows typical steady-state emission spectra for 100 μM pyrene in liquid methanol (MeOH) and acetonitrile (MeCN). The I_1/I_3 are 1.39 and 1.80 for liquid MeOH and MeCN, respectively. When pyrene is promoted to the excited state there is a temporary dipole established in the molecule.[44] As a result, dipole–dipole interactions between the excited singlet state of pyrene and the solvent result in enhanced

(54) Beecham, J. M.; Ameloot, M.; Brand, L. *Chem. Phys. Lett.* **1985**, *120*, 466.
(55) Beecham, J. M.; Ameloot, M.; Brand, L. *Anal. Instrum. (N.Y.)* **1985**, *14*, 379.
(56) Ameloot, M.; Boens, N.; Andriessen, R.; Van den Bergh, V.; De Schryver, F. C. *J. Phys. Chem.* **1991**, *95*, 2041.
(57) Andriessen, R.; Boens, N.; Ameloot, M.; De Schryver, F. C. *J. Phys. Chem.* **1991**, *95*, 2047.
(58) Barrow, G. M. *Physical Chemistry*, 4th ed.; McGraw-Hill: New York, 1979; Chapter 19.
(59) Betts, T. A.; Bright, F. V. *Appl. Spectrosc.* **1990**, *44*, 1196.
(60) Betts, T. A.; Bright, F. V. *Appl. Spectrosc.* **1990**, *44*, 1204.
(61) Angus, A.; Armstrong, B.; de Reuck, K. M. *International Thermodynamic Tables of the Fluid State Carbon Dioxide*, Pergamon Press: New York, 1976.
(62) Golubev, I. F.; Petrov, V. A. *Trudy GIAP* **1953**, *2*, 5.

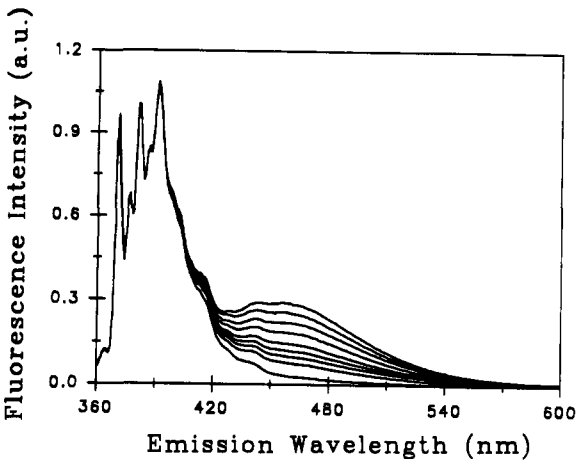

Figure 4. Steady-state emission spectra for 100 μM pyrene in sub- and supercritical CO_2. T = 40 °C; pressure range = 86–117 bar. λ_{ex} = 337 nm; excitation spectral bandpass = 16 nm; emission spectral bandpass = 2 nm. The excimer emission is decreasing with increasing pressure.

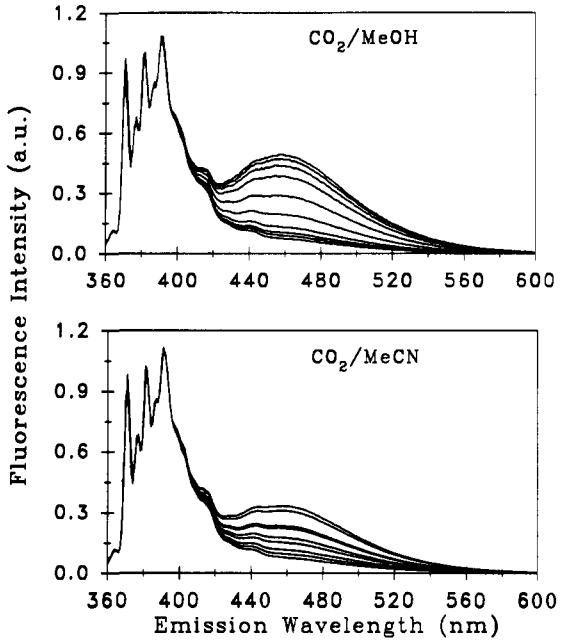

Figure 5. Steady-state fluorescence emission spectra for 100 μM pyrene in sub- and supercritical Co_2/MeOH and Co_2/MeCN. T = 40 °C; pressure range = 86–172 bar. λ_{ex} = 337 nm; excitation spectral bandpass = 16 nm; emission spectral bandpass = 2 nm. The excimer emission is decreasing with increasing pressure.

intensity in the first vibronic peak. Because MeCN has a larger dipole moment (3.92 vs 1.63 D), greater enhancement is observed.

Figures 4 and 5 show a series of density-dependent emission spectra obtained at 40 °C for 100 μM pyrene in pure and entrainer-modified CO_2, respectively. The analytical concentration of MeOH and MeCN is 9.89×10^{-2} and 7.66×10^{-2} M, respectively, and remains constant throughout a given experiment. This dilute concentration of entrainer does not significantly alter the critical properties or density of the binary solvent mixture.[7]

The effects of fluid density, temperature, and entrainer on the pyrene I_1/I_3 ratios are plotted in Figure 6. As expected, this ratio is lowest in pure CO_2 (lower panel). Upon addition of entrainer (upper and center panels), I_1/I_3 shifts between pure CO_2 (lower panel) and pure entrainer (Figure 3). Thus, the small amount of added entrainer results in an environment which is neither completely polar nor nonpolar. On the basis of the liquid results (Figure 3), one would anticipate the I_1/I_3 ratio in CO_2/MeCN to be greater than CO_2/MeOH. However, one sees experimentally that these two entrainers act similarly. This implies that the local environments surrounding pyrene are nearly the same in CO_2/MeOH and CO_2/MeCN.[63] From these results one can envision

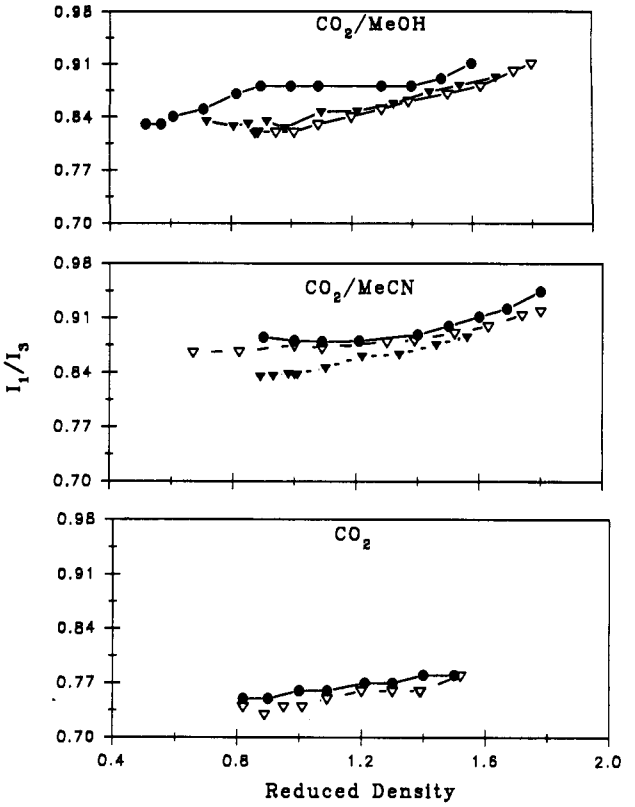

Figure 6. Ratio of the first vibronic peak (I_1, 367–374 nm) to the third vibronic peak (I_3, 379–384 nm) for pyrene in supercritical Co_2/MeOH (upper panel), Co_2/MeCN (center panel), and CO_2 (lower panel) as a function of reduced density (symbol, temperature): (●, 35 °C); (▽, 40 °C); (▲, 47 °C).

two scenarios. First, there may be more MeOH molecules involved in the local solute–fluid cluster compared to MeCN. Second, the average orientation of the MeOH entrainers (about pyrene) may be more effective at coupling with the temporary excited-state dipole. Thus, one could envision the case where more MeCN molecules are about pyrene but the MeOH are more efficiently oriented to interact with the solute temporary dipole.

Excimer emission is not observed for 100 μM pyrene in normal liquids (Figure 3) but is prominent in supercritical solvents (Figures 4 and 5). One can follow the efficiency of excimer formation by monitoring the amount of excimer relative to monomer (I_{ex}/I_{mon}). This ratio is plotted in Figure 7 as a function of CO_2 density and temperature. There are two interesting features associated with these results. First, the relative amount of excimer formed in entrainer-modified CO_2 is significantly greater than that formed in pure CO_2, and it is greatest for the CO_2/MeOH system. This result is interesting because similar work in CF_3H showed that there was significant solute–fluid interactions ($I_1/I_3 > 1$) but low levels of excimer.[49] Second, the fraction of excimer formed in pure and entrainer-modified CO_2 decreases significantly with increasing density.

Time-resolved fluorescence spectroscopy is necessary to further interpret these experimental results.[48] However, prior to proceeding we must determine the composition of the pyrene ground electronic state because multiple species (e.g. pyrene monomer and dimer) would complicate the photophysics (i.e., Figure 1 would not be accurate). Emission wavelength-dependent excitation spectra[48,64] are used to probe the ground state. Figure 8 shows

(63) Additional experiments were conducted to determine how the concentration of entrainer affected I_1/I_3. 5, 10 and 20 μL injections of each entrainer were added and the steady-state emission spectra recorded. The I_1/I_3 ratio did not significantly change as the entrainer concentration was varied. This suggests that the local environment about pyrene is "saturated" with entrainer even at 1 mol %.

(64) Yorozu, T.; Hoshino, M.; Imamura, M. *J. Phys. Chem.* **1982**, *86*, 4426.

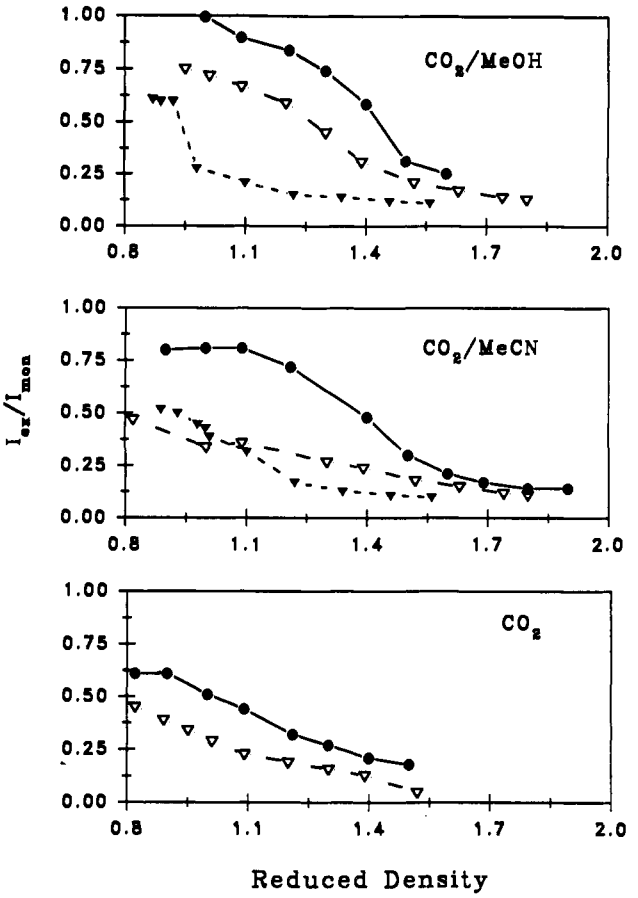

Figure 7. Relative amount of pyrene excimer as a function of fluid temperature and reduced density in supercritical CO_2/MeOH (upper panel), CO_2/MeCN (center panel), and CO_2 (lower panel). The expression I_{ex}/I_{mon} is the ratio of excimer-to-monomer. The terms I_{ex} and I_{mon} denote the areas between 440–500 and 367–420 nm, respectively. The measurement imprecision in I_{ex}/I_{mon} is about the size of the data points themselves (symbol, temperature): (●, 35 °C); (▽, 40 °C); (▲, 47 °C).

Table I. Experimentally Recovered and Theoretical Values for the Forward Bimolecular Rate Coefficient (k_{DM}) for Pyrene Excimer Formation in Supercritical CO_2/MeOH[a,b]

pressure (bar)	$10^{11}k_{DM}$(ex) (M^{-1} s^{-1})	$10^{11}k_{DM}$(th) (M^{-1} s^{-1})[c]
	T = 35 °C	
80.0	0.44	2.7
80.7	0.81	2.0
90.3	0.79	1.4
148.2	0.79	1.1
	T = 40 °C	
88.6	1.5	1.9
89.3	1.6	1.7
103.4	1.3	1.3
172.4	1.1	1.2
	T = 47 °C	
99.3	2.4	2.6
203.0	2.4	2.1
125.5	2.2	1.8
202.0	1.2	1.4

[a] Experiments were performed by maintaining the corresponding temperature and adjusting the pressure. Fluorescence decays were obtained at three different wavelengths for two different pyrene concentrations. The rate coefficients were recovered by linking the spectral parameters over the entire multidimensional data surface.[86,87] [b] Uncertainties in recovered rates ≤15%. [c] Calculated from the Smoluchowski equation (eq 1) using viscosities for pure CO_2.

a typical set of spectra for 100 μM pyrene in CO_2/MeOH and CO_2/MeCN. Similar results are seen at all temperatures and densities studied (not shown). These results are consistent with

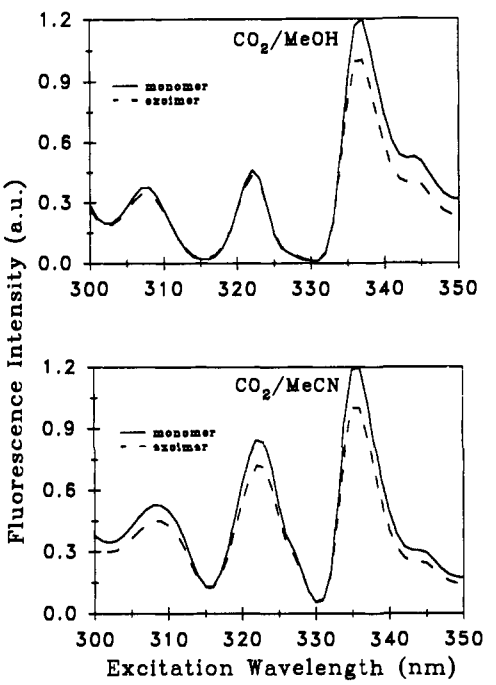

Figure 8. Normalized, emission wavelength-dependent steady-state excitation spectra for 100 μM pyrene in supercritical CO_2/MeOH and CO_2/MeCN at 40 °C and a pressure of 89 bar. The spectra indicated as monomer and excimer were acquired at λ_{em} = 380 and 460 nm, respectively. Excitation spectral bandpass = 2 nm; emission spectral bandpass = 16 nm. The entire monomer spectrum is purposefully offset for clarity.

Table II. Experimental Unimolecular Rates for Pyrene in Supercritical CO_2/MeOH[a,b]

pressure (bar)	10^9k_{MD} (s^{-1})	10^6k_M (s^{-1})	10^6k_D (s^{-1})
	T = 35 °C		
80.0	0.38	2.8	2.0×10^{-2}
80.7	0.51	3.3	2.0×10^{-2}
90.3	1.3	3.1	4.0×10^{-2}
148.2	2.9	3.4	5.0×10^{-2}
	T = 40 °C		
88.6	1.1	3.0	3.0×10^{-2}
89.3	0.92	2.7	7.0×10^{-2}
103.4	0.86	2.5	2.0×10^{-2}
172.4	1.0	2.7	1.0×10^{-2}
	T = 47 °C		
99.3	3.6	2.7	7.0×10^{-2}
102.0	6.2	3.0	1.2×10^{-3}
125.5	7.2	2.9	1.3×10^{-3}
202.0	7.2	2.6	1.3×10^{-3}

[a] Same experimental procedure as described in Table I. [b] Uncertainties in recovered rates ≤15%.

no excimer-like pyrene preassociation existing in the ground state; the model presented in Figure 1 is valid.

Time-Resolved Experiments. To determine how entrainer-modified supercritical CO_2 affects the pyrene photophysics we acquired time-resolved decay traces over a broad range of pyrene concentrations, fluid densities, and temperatures. Figures 9 and 10 show typical fluorescence intensity decay traces for 100 μM pyrene in CO_2/MeOH and CO_2/MeCN, respectively. The lower and upper panels illustrate the results recovered for selective observation of the monomer (400 nm) and excimer (480 nm) emission in the near-critical region. The scatter traces were obtained by monitoring the Rayleigh scattered laser line. The sought after rate terms (Figure 1) are recovered by simultaneous global analysis[54-57] of multiple fluorescence decay experiments.[48,49] These results are summarized in Tables I–IV.

Tables I and III present the experimentally recovered bimolecular rate coefficients for pyrene excimer formation (k_{DM}) as a function of fluid density and temperature for CO_2/MeOH and

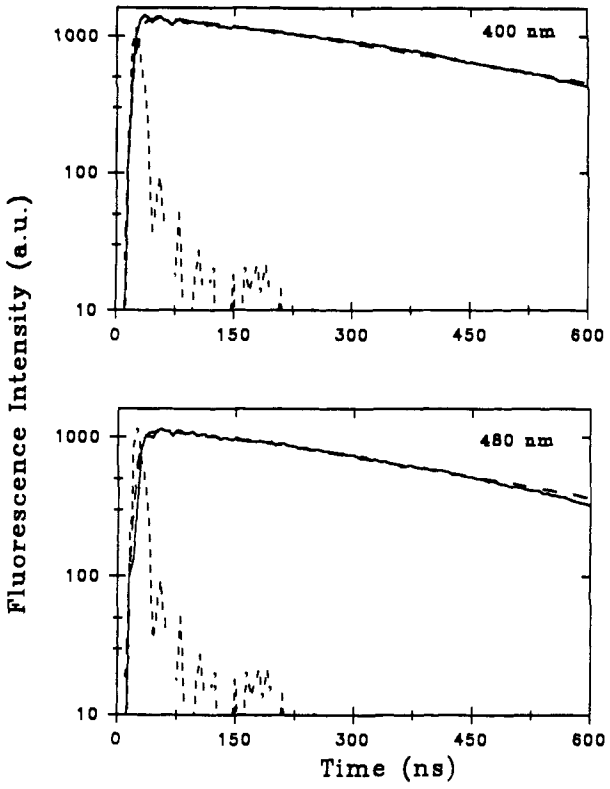

Figure 9. Typical time-resolved fluorescence decay traces for 100 μM pyrene in supercritical CO_2/MeOH. T = 40 °C and P = 89 bar. Upper and lower panels represent monomer (400 nm) and excimer (480 nm) emission, respectively: (—) experimental decay; (– – –) fit; (- - -) scatter.

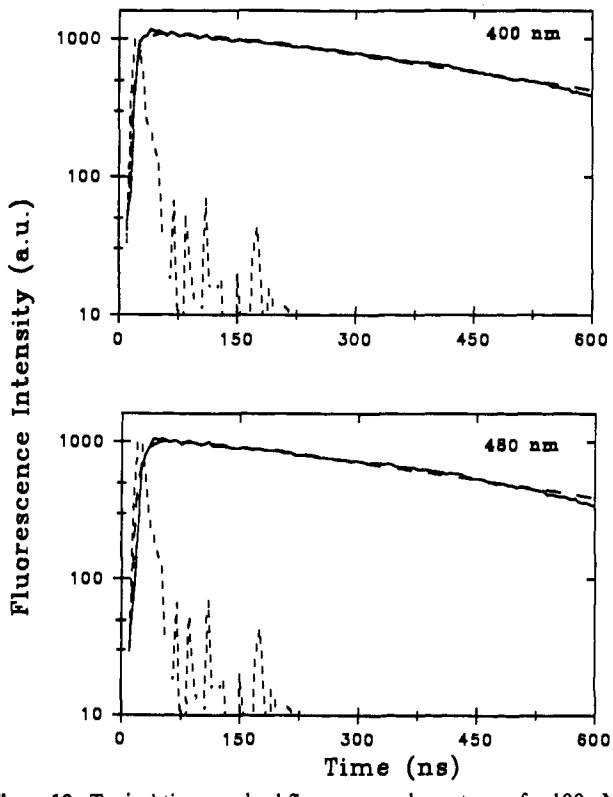

Figure 10. Typical time-resolved fluorescence decay traces for 100 μM pyrene in supercritical CO_2/MeCN. T = 47 °C and P = 102 bar. Upper and lower panels represent monomer (400 nm) and excimer (480 nm) emission, respectively: (—) experimental decay: (– – –) fit; (- - -) scatter.

CO_2/MeCN. Also shown are the predicted rate coefficients based on diffusion control (eq 1). Inspection of these results reveals several interesting trends. For example, the deviation from the predicted diffusion-controlled model is evident in both entrainer systems. That is, the excimer formation reaction proceeds *slower* than expected. We also see that the pyrene excimer formation rate is slowest in the CO_2/MeOH system. As stated previously, the pyrene excited state results in a short-lived dipole[44] which in turn leads to temporary dipole–dipole coupling between excited-state pyrene and the polar entrainers (Figures 3–6). From time-resolved fluorescence, we see that these strong–entrainer interactions affect the excited-state reaction by slowing the rate of excimer formation (Tables I and III). This result is reminiscent of those seen in CF_3H[49] and is consistent with the entrainer/CO_2 cluster[65] shielding pyrene and precluding excimer formation. Finally, as we move away from the critical point, by increasing temperature and/or pressure, the excimer formation process once again becomes diffusion controlled. Together these results are consistent with (1) clustering markedly affecting the excimer

Table III. Experimentally Recovered and Theoretical Values for the Forward Bimolecular Rate Coefficient (k_{DM}) for Pyrene Excimer Formation in Supercritical CO_2/MeCN[a,b]

pressure (bar)	$10^{11}k_{DM}$(ex) (M^{-1} s^{-1})	$10^{11}k_{DM}$(th) (M^{-1} s^{-1})[c]
	T = 35 °C	
80.0	1.6	2.7
80.7	1.1	2.0
90.3	0.63	1.4
148.2	0.71	1.1
	T = 40 °C	
88.6	1.7	1.9
89.3	0.50	1.7
103.4	0.60	1.3
172.4	0.60	1.2
	T = 47 °C	
99.3	2.9	2.6
102.0	1.1	2.1
125.5	1.1	1.8
202.0	1.1	1.4

[a] Experiments were performed by maintaining the corresponding temperature and adjusting the pressure. Fluorescence decays were obtained at three different wavelengths for two different pyrene concentrations. The rate coefficients were recovered by linking the spectral parameters over the entire multidimensional data surface.[86,87] [b] Uncertainties in recovered rates ≤15%. [c] Calculated from the Smoluchowski equation (eq 1) using viscosities for pure CO_2.

Table IV. Experimental Unimolecular Rates for Pyrene in Supercritical CO_2/MeCN[a,b]

pressure (bar)	10^9k_{MD} (s^{-1})	10^6k_M (s^{-1})	10^6k_D (s^{-1})
	T = 35 °C		
80.0	1.5	1.4	0.18
80.7	1.4	1.5	0.11
90.3	1.2	1.7	3.6
148.2	9.4	1.5	25
	T = 40 °C		
88.6	1.7	2.3	2.9
89.3	1.9	1.9	3.8
103.4	5.6	0.80	1.3×10^2
172.4	6.1	0.71	1.5×10^2
	T = 47 °C		
99.3	6.6	0.89	2.9×10^2
102.0	14	0.56	2.1×10^3
125.5	14	0.42	3.0×10^3
202.0	10	1.2	1.7×10^3

[a] Same experimental procedure as described in Table I. [b] Uncertainties in recovered rates ≤15%.

(65) Throughout the text we continually refer to the term cluster. This word choice is mostly pedagogical, but the reader should realize that this term is used to define a situation in which the local solvent composition about the solute exceeds, *on average*, that of the bulk. Molecular dynamics simulations[26] show the dynamical nature of these clusters.

formation reaction rate in the near-critical region and (2) these clusters coalescing into the bulk fluid as temperature and pressure are increased.

Clustering affects not only the rate of excimer formation but also the other kinetic terms (Table II and IV). For example, in the near-critical region the excimer emissive decay rate is significantly slower than at higher temperatures and pressures. It is also slower in CO_2/MeOH compared to CO_2/MeCN. This is a strong indication that the excimer excited state is stabilized (protected from nonradiative pathways) significantly near the critical point. The fact that the CO_2/MeOH has a greater stabilizing affect compared to CO_2/MeCN may be a consequence of differences in the size of the cluster (vide supra).

Comparing the rates of excimer formation and dissociation between CO_2/MeOH and CO_2/MeCN (Tables II and IV) it is apparent that the entrainers affect the reaction differently. For example, the rate of excimer formation is, in general, slower and the rate of excimer dissociation faster in CO_2/MeCN compared to CO_2/MeOH. When an excited- and ground-state monomer react in the excited state, a net excited-state dipole moment of zero is established in the excimer and there is a rapid and significant change in solute–fluid interactions. That is, once the excimer forms there is no longer any possibility for temporary dipole–dipole interactions (between the excimer and entrainer); only induced dipoles contribute. Thus, the enhanced dipole–dipole interactions which result in the stronger coupling of MeCN (Figure 3) with excited-state pyrene monomer are not found with the excimer, and without the added strength offered by hydrogen bonding, the pyrene–CO_2/MeCN cluster apparently weakens. This accounts for the slower rate of excimer formation and the faster rate of excimer dissociation in CO_2/MeCN compared to CO_2/MeOH.

As seen previously,[48,49] the rate of excimer dissociation and the emissive decay rate simultaneously increase with density which accounts for the decrease in the steady-state excimer emission contour. Once again, the monomer emissive decay rate (k_M) is essentially unaffected by temperature and density. This rate is slowest in CO_2/MeCN compared with any of the other fluid systems studied, also indicating that MeCN interacts more strongly with the excited-state pyrene monomer.

Conclusions

We report on the steady-state and time-resolved fluorescence of pyrene in binary supercritical fluids composed of CO_2 and MeCN or MeOH. Pyrene is a nearly ideal probe because it provides simultaneous information on solute–fluid and solute–solute interactions. Specifically, the static monomer emission gives insight into solute–fluid interactions and the time-resolved data provide information on solute–solute interactions and the overall system kinetics.

Our steady-state and time-resolved fluorescence show that there is no ground-state, excimer-like preassociation of pyrene molecules in either pure[48,49] or entrainer-modified supercritical fluids (this work) over the concentration range studied (up to 100 μM). Thus, the solute–fluid clusters (heteroclusters is probably a better term in the current work) are of such a nature that they do not force pyrene monomers to form an excimer-like dimer in the ground state.

The I_1/I_3 ratio confirms increased interactions in the entrainer-modified CO_2 versus pure CO_2; however, I_1/I_3 values are nearly equal in CO_2/MeOH and CO_2/MeCN. This indicates that the environments surrounding the pyrene monomer are similar at this concentration level. Because MeCN is significantly more polar than MeOH, this is consistent with more MeOH molecules being involved (compared to MeCN) in the cluster or the permanent dipole in MeOH being more effectively aligned relative to the temporary dipole of pyrene and maximizing pyrene–entrainer interaction.

The excimer dissociation and emissive rates in CO_2/MeOH are slower which is somewhat consistent with the larger cluster argument. This supports stronger interaction between the binary fluid (CO_2/MeOH) and the excimer. For CO_2/MeCN, the monomer emissive rate and the rate of excimer formation are slower than those observed in CO_2/MeOH. This supports stronger interaction between the binary fluid (CO_2/MeCN) and the monomer. By comparing the two systems, it is evident that the potential to hydrogen bond between entrainer molecules, and solute–entrainer interactions (i.e., dipole–dipole), plays a key role in cluster formation. Specifically, CO_2/MeOH interacts more strongly with pyrene excimer, CO_2/MeCN interacts more strongly with pyrene monomer, and both systems interact with the excimer more than has been reported in any supercritical fluid.[48,49]

Finally, clustering in entrainer-modified CO_2 affects the bimolecular rate of excimer formation. In the near-critical region the recovered rate is less than predicted based on diffusion control and indicates that the solute–fluid cluster precludes excimer formation.

Acknowledgment. This work has been generously supported by the United States Department of Energy (DE-FG02-920ER14143). Further appreciation is extended by Gary Sagerman for his continued help with instrument design and construction. We also thank Ming Li and Michaleen Pacholski for the spectrum of pyrene in acetonitrile.